Electronic Supplementary Material (ESI) for Nanoscale.

Supporting Information

Corresponding Author: **spad@iacs.res.in** Phone: +91-33-24734971.

Screening Two Dimensional Materials for the Transportation and Delivery of Diverse Genetic Materials

Titas Kumar Mukhopadhyay, Ayan Datta*

School of Chemical Sciences, Indian Association for the Cultivation of Science, 2A and 2B Raja S.C.Mullick Road, Jadavpur, Kolkata-700032, West Bengal, India.

Contents:

18. Analyses of normalized dynamical properties during DNA adsorption on 2D materials.

19. Accuracy of simulations and comparison with AMBER parameters.

20. Principal Component Analysis of the dsDNA and GQ adsorption on 2D materials.

1. Minimization – equilibration protocol for the simulations performed:

First, each of the systems was minimized for 10000 steps while keeping the DNA atoms constrained by a harmonic force constant of 100 kcal/mol/Å2 and another minimization was performed for 10000 steps without any constraint. Then, the systems were equilibrated for 20 ns at 100 K in canonical (NVT) ensemble, again constraining the DNA atoms by a force constant of 100 kcal/mol/Å2. Further, the force constant was reduced to 10 kcal/mol/Å2 and heating was performed to 300 K over the period of 20 ns. Finally, constraining forces over DNA atoms were removed and the systems were equilibrated for another 20 ns in isothermal – isobaric (NPT) ensemble at 300 K and 1 atmospheric pressure. In all the above simulations, each C_2N atom was harmonically constrained by a force constant of 200 kcal/mol/ $Å^2$. Finally, production simulations were carried out with structures obtained at the end of the equilibration simulations using two different initial configurations for each system, at 300 K in NVT ensemble. Also, for the simulations of DNA in the absence of 2D materials, the above mentioned protocol was followed for minimization as well as equilibration and production simulations. It should be noted that, in many of the additional sets of simulations (Simulations 1(b), 2(b), 3(b), 12(a), 14(b), 15(b)) we continued the production simulations in NPT ensemble. Nevertheless, we did not observe any changes in the trends of the results found and in all the cases adsorption on C_2N lead to little to no disruption of the nucleic acid structure while adsorption on graphene and *h*-BN lead to complete disruption of ssDNA and GQ (1KF1) as well as UBP containing dsDNA.

2. Computational procedure for PMF calculations:

For the calculation of 1D PMF's, center of mass (COM) distances (d) between the DNA and the 2D materials are chosen as the reaction coordinates which are divided into several overlapping windows of 0.1 nm widths. Each of these windows is further divided into small bins of 0.2 nm widths. A harmonic force of 100 kcal/mol/Å is applied to the upper and lower boundaries of the reaction coordinates in all the windows. Finally, a 3 ns production ABF simulation is performed for each window at 300 K using NVT ensemble. To reduce sampling issues and obtain sufficient consistency in the calculated binding free energy trends, we performed each PMF calculations for at least two times with two different adsorbed structures obtained from two separate production simulations and averages are reported. The DNA's are adsorbed at different COM distances with respect to the 2D materials and for a direct comparison between the PMF curves, we substituted the reaction coordinate d with δ, where δ is defined as $(d - d_0)$, d_0 and d being the COM distances initially and at any instant during PMF calculations respectively. Free energy of the completely desorbed structure is set to zero, where DNA's are non-interacting with the surfaces.

On the other hand, for 2D - PMF calculations, a single strand of the mononucleotide dA is prepared and allowed to adsorb over C_2N, graphene and *h* – BN surfaces respectively in presence of water and 0.15 molar NaCl at 300 K for 60 ns. The projection of COM distances between the mononucleotide and the 2D materials along x (d_x) and y axes (d_y) are chosen as the simultaneous reaction coordinates and they are varied from 0 to 1.2 nm. Each of the reaction coordinates are simultaneously divided into windows of 0.2 nm width and simulations are performed for each window for at least 20 ns. For the construction of free energy landscapes, the discretized gradients are integrated using the "abf_integrate" utility implemented in NAMD2.12 which executes a Monte – Carlo (MC) simulation in collective variable space utilizing a history

dependent bias. This bias counteracts with the gradient after convergence and is negated for the construction of the free energy landscape.

3. Decomposition of the ssDNA – C_2N interaction energies for two sets of simulations:

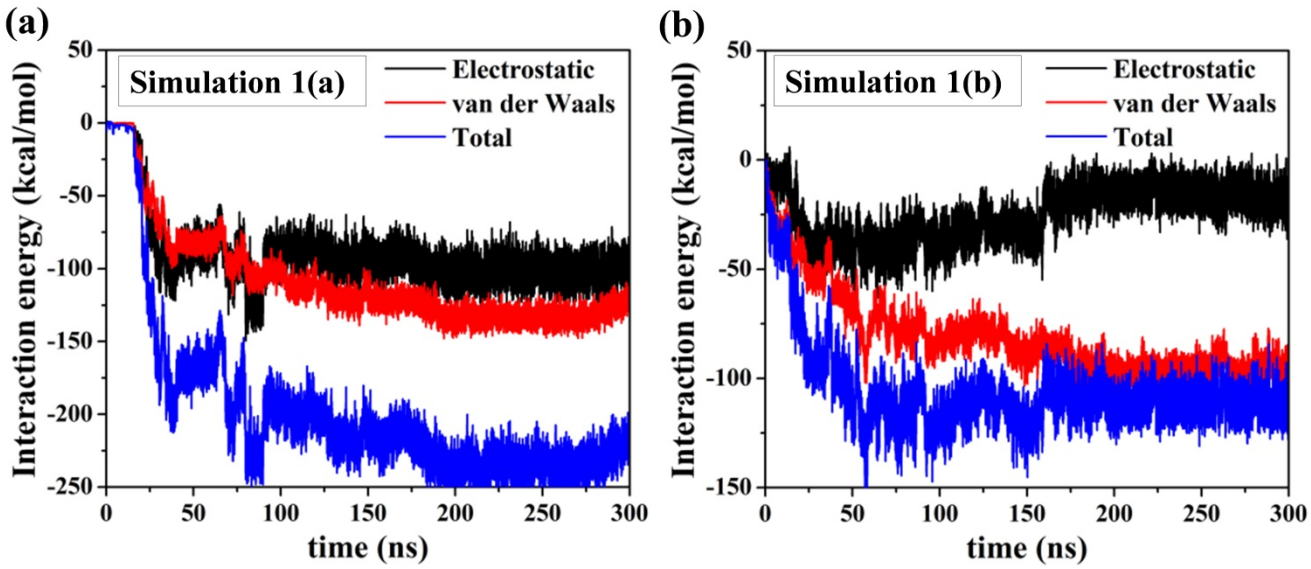

Figure S1: Decomposition of ssDNA-C_2N interaction energy into electrostatic and van der Waals components for (a) simulation 1(a) and (b) simulation 1(b).

4. Analyses of the second set of simulations for the adsorption of ssDNA on 2D materials:

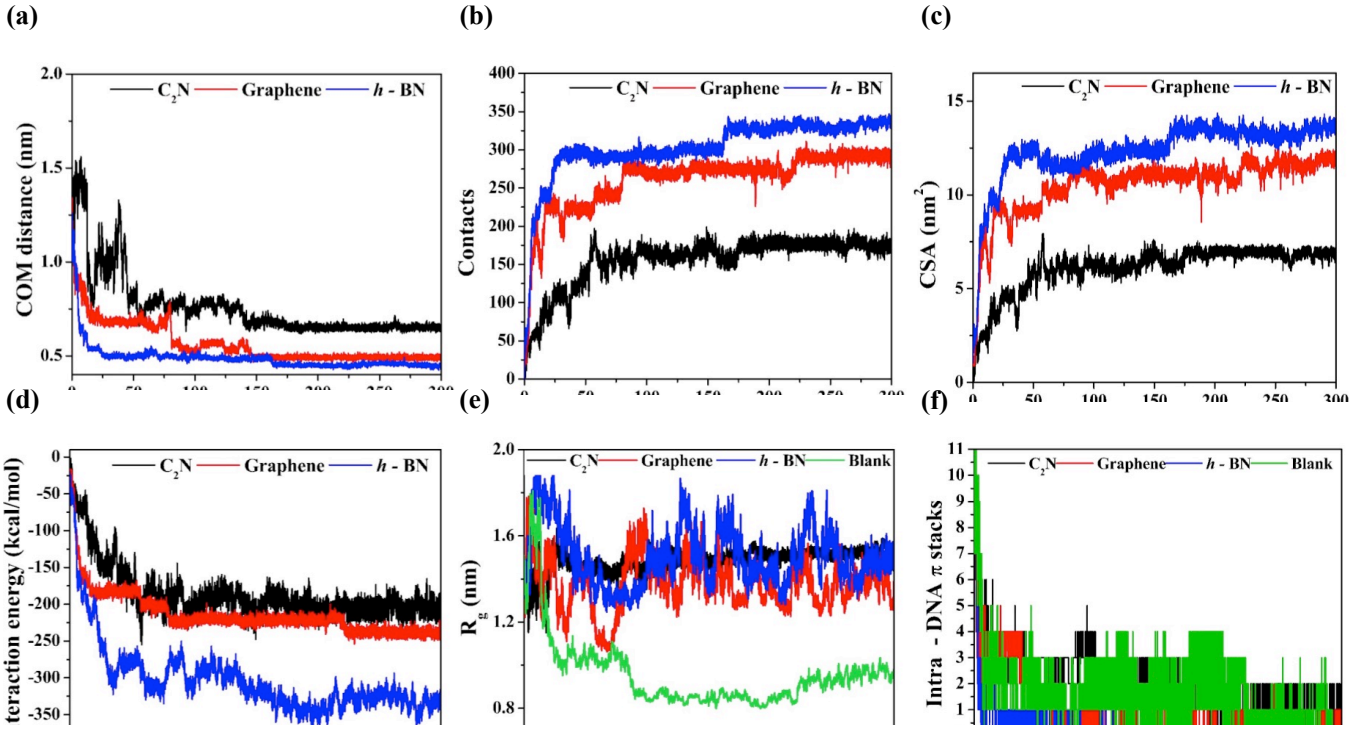

Figure S2: *Time evolution of various dynamical quantities characterizing the adsorption of ssDNA onto C_2N, graphene and h – BN: (a) COM distance, (b) number of contacts (N_c), (c) contact surface area(CSA), (d) interaction energy, (e) radius of gyration (R_g) of ssDNA and (f) intra – ssDNA sequential π stacking contacts.*

5. Snapshots of the 2D material mediated unwinding of DNA double helix:

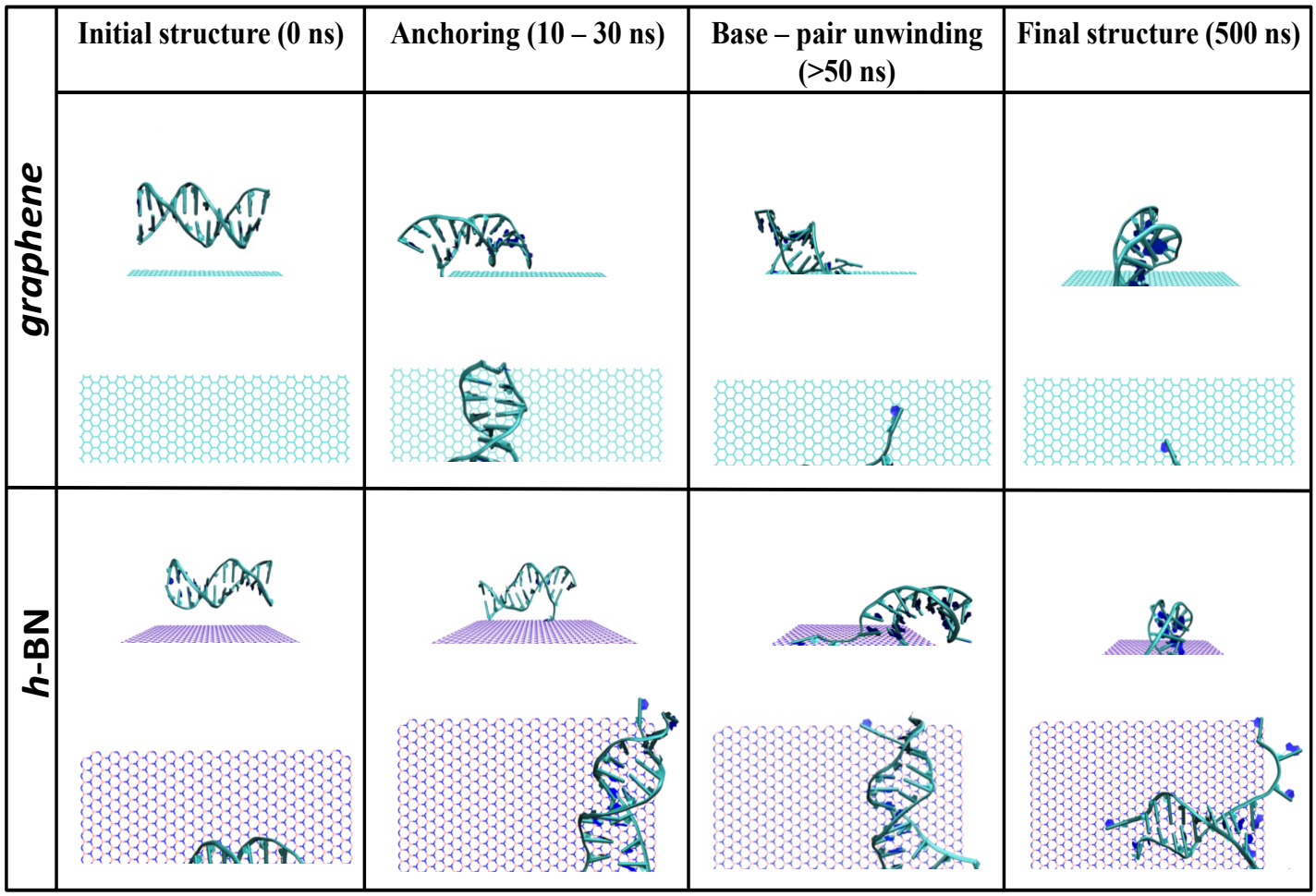

FigureS3

: *Snapshots corresponding to the side and top views of dsDNA adsorption on graphene and h – BN, clearly depicting the hierarchical steps for 2D material mediated dsDNA unwinding. Note*

that, at the end of 500ns, all Watson – Crick base pairs are not cleaved, thereby suggesting a thermodynamically feasible but kinetically sluggish pathway for dsDNA unwinding.

6. Analyses of simulations for the adsorption of a dsDNA on three 2D materials:

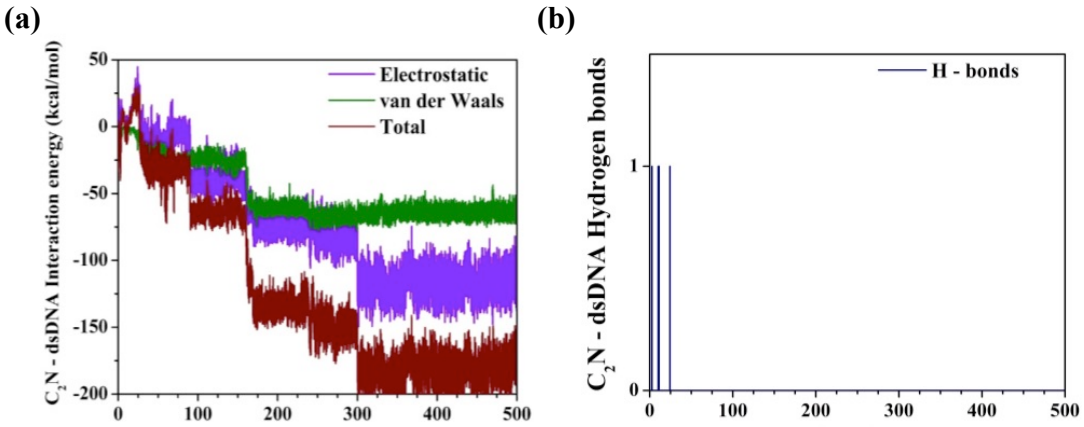

Figure S4: *Time evolution of various dynamical quantities characterizing the adsorption of dsDNA onto C_2N: (a) decomposition of the C_2N – dsDNA interaction energy into electrostatic and van der Waals components and (b) number of C_2N – dsDNA H – bonds.*

7. Molecular structures of d5SICS-dNaM:

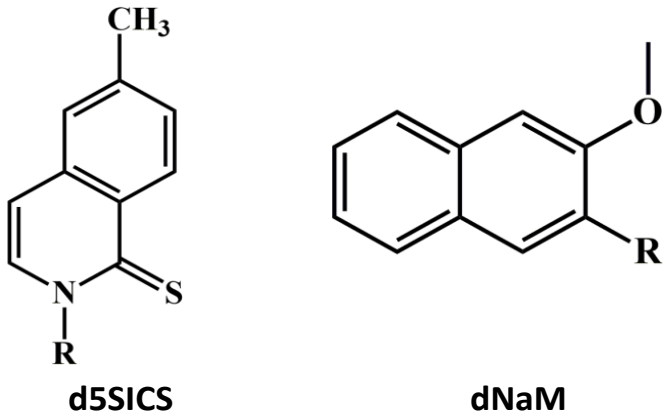

Figure S5: *Molecular structures of unnatural bases d5SICS and dNaM used in this study to test the stability of UBP substituted dsDNA.*

8. Analyses of simulations for the adsorption and stabilization of three pairs of UBP (d5SICS – dNaM) substituted 11 mer of a dsDNA on three 2D materials:

In recent years, the urge to expand the genetic alphabets beyond the natural ones have generated considerable interest concerning the stabilization of unnatural base pair (UBP) containing DNA. Romesberg and coworkers have demonstrated a synthetic design of *E. coli* bacteria containing complementary unnatural nucleobases d5SICS and dNaM within the DNA to replicate under intracellular conditions.[1-3] In fact, a series of unnatural nucleobases capable of mimicking the natural ones, have been synthesized and predicted to give substantial stability to the double helical form, albeit being less stable than the natural canonical congeners.[3,4] The reductions in the stability of the dsDNA upon UBP substitution have been attributed to the replacement of inter – strand WC H – bonding between canonical base pairs by weaker van der Waals interactions. To check if the ability of C_2N to adsorb dsDNA without structural perturbation is maintained in case of a less stable dsDNA comprising of few UBP's, we performed additional 300 ns adsorption simulations with a 3 UBP (d5SICS – dNaM) substituted 11 bp long dsDNA. Also, simulations on graphene and h – BN are performed for comparison. The results (Figure S5) altogether indicate that, while graphene and h – BN easily breaks the interactions between weakly bound polynucleotide strands, C_2N completely preserves it (Figure 4). Rather, we observe reorganization of the dsDNA after adsorption, characterized by the formation of new WC H – bonding between two strands involving nucleobases which are previously disrupted due to the introduction of UBP's as well as adsorption. Thus, we propose that, C_2N may certainly be used for the preservation and transportation of dsDNA of any kind, even for relatively unstable sequences.

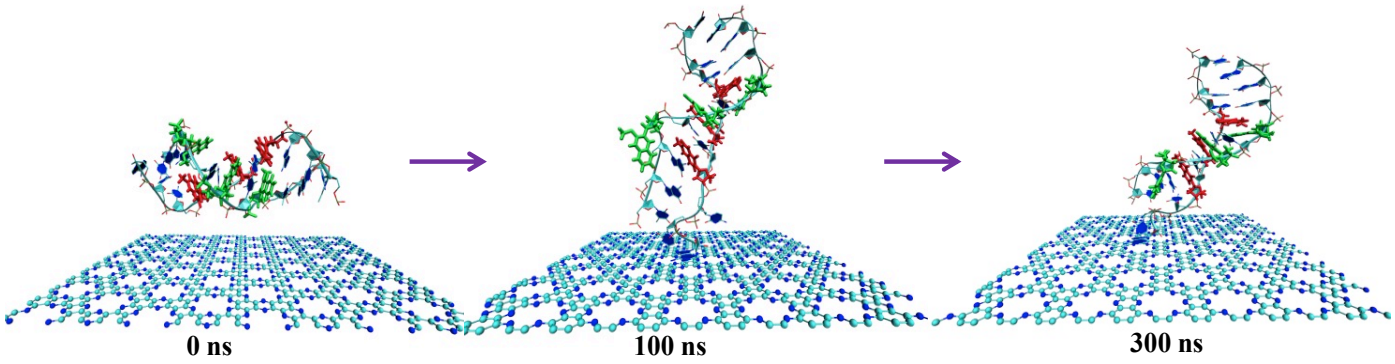

Figure S6: *Snapshots for the adsorption of a 3 unnatural base pair (d5SICS – dNaM) containing 11 base pair long dsDNA over C_2N at different time instants. Unnatural bases d5SICS and dNaM are labeled using red and green colors respectively. It is clearly seen that, even after 300ns, the structural integrity of the UBP substituted dsDNA is maintained and it remains nearly perpendicular to C_2N, being adsorbed only through terminal nucleobase pairs.*

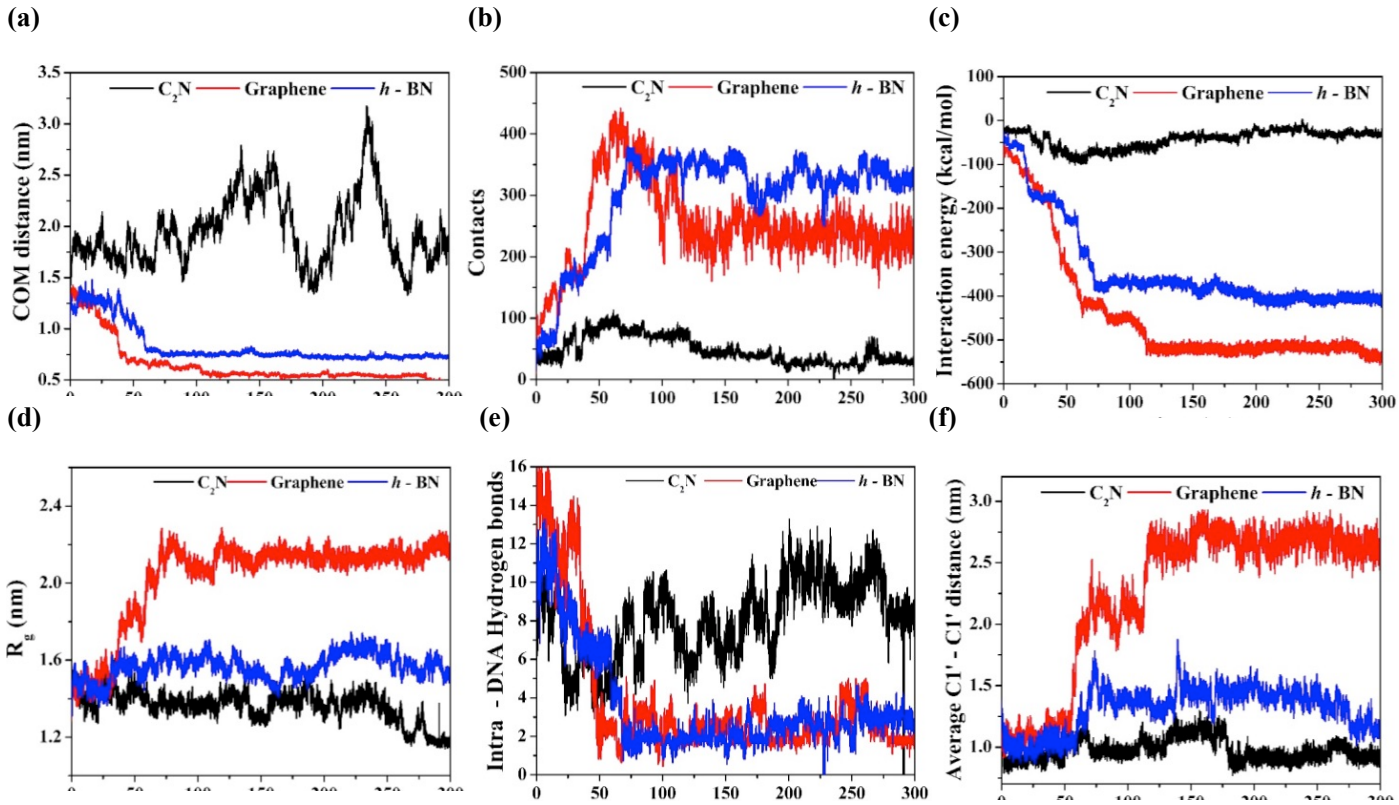

Figure S7: *Time evolution of various dynamical quantities characterizing the adsorption of a 3 – UBP substituted dsDNA onto C_2N, graphene and h – BN: (a) COM distance, (b) number of*

contacts (N_c), (c) interaction energy, (d) radius of gyration (R_g) of ssDNA, (e) intra – dsDNA WC H – bonds and (f) average C1' – C1' distance of the three UBP's.

9. Analyses of simulations for the adsorption and stabilization of three pairs of UBP (d5SICS – dNaM) substituted 12 mer of a dsDNA on *h*2D-C_2N:

We have also selected the Dickerson – Drew Dodecamer dsDNA sequence and inserted three UBP's. Since graphene and h-BN are able to disrupt any of the dsDNA sequences, therefore, we only selected C2N as the substrate. Two 600 ns long simulations are performed with the 12 mer dsDNA of which one resulted in the flipping of the dsDNA to yield a perpendicular structure, similar to that obtained for the dsDNA without UBP and the 11 mer dsDNA containing 11 UBP. Through preliminary structural and visual analysis, we observed no structural destabilization of the nucleic acid structure and it had very few contacting residues with the 2D material beneath. Interestingly, the other simulation yielded a parallely adsorbed dsDNA without any flipping event. Since this observation is unique and the parallel mode of adsorption can lead to stronger interaction with the surface, therefore, we performed detailed analysis of this particular simulation and the results are reported in Figure S8 of the supporting information file. As observed from Figure S8(a), after initial fluctuation, the dsDNA gradually comes close to the surface and gets adsorbed. No further fluctuation in the centre of mass distance between the dsDNA and C2N clearly indicates absence of the flipping event. However, even after adsorbing in a parallel geometry, the equilibrated number of contacts with the surface (Figure S8(b)) is not much high, suggesting significantly weak interaction with the nucleic acid. The same conclusion can be drawn from the interaction energy also (Figure S8(c)). Furthermore, time evolution of different dynamical quantities such as R_g, average C1'-C1' distance and the intra-DNA hydrogen bonds (Figures S8(d-f)) evidently demonstrates conservation of the native structure without

much perturbation. Therefore, the results obtained for both the 11mer and 12 mer dsDNA are commensurate with each other, confirming the stability of UBP substituted duplex DNA's upon adsorption on C2N.

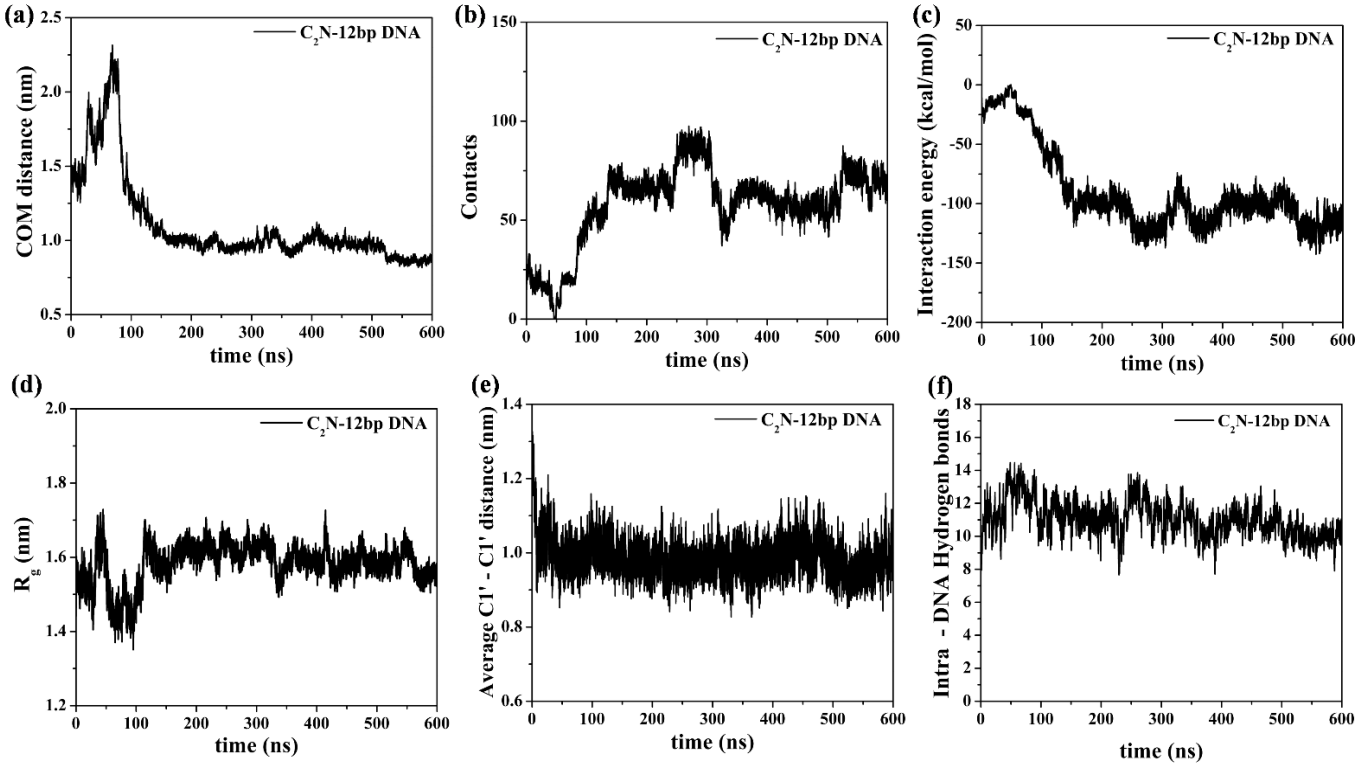

Figure S8: *Time evolution of various dynamical quantities characterizing the adsorption of a 3 – UBP substituted 12 mer of a dsDNA onto C_2N: (a) COM distance, (b) number of contacts (N_c), (c) interaction energy, (d) radius of gyration (R_g) of dsDNA, (e) intra – dsDNA WC H – bonds and (f) average C1' – C1' distance of the three UBP's.*

10. Analyses of the 1microsecond long adsorption simulation of 1KF1 – GQ on C_2N:

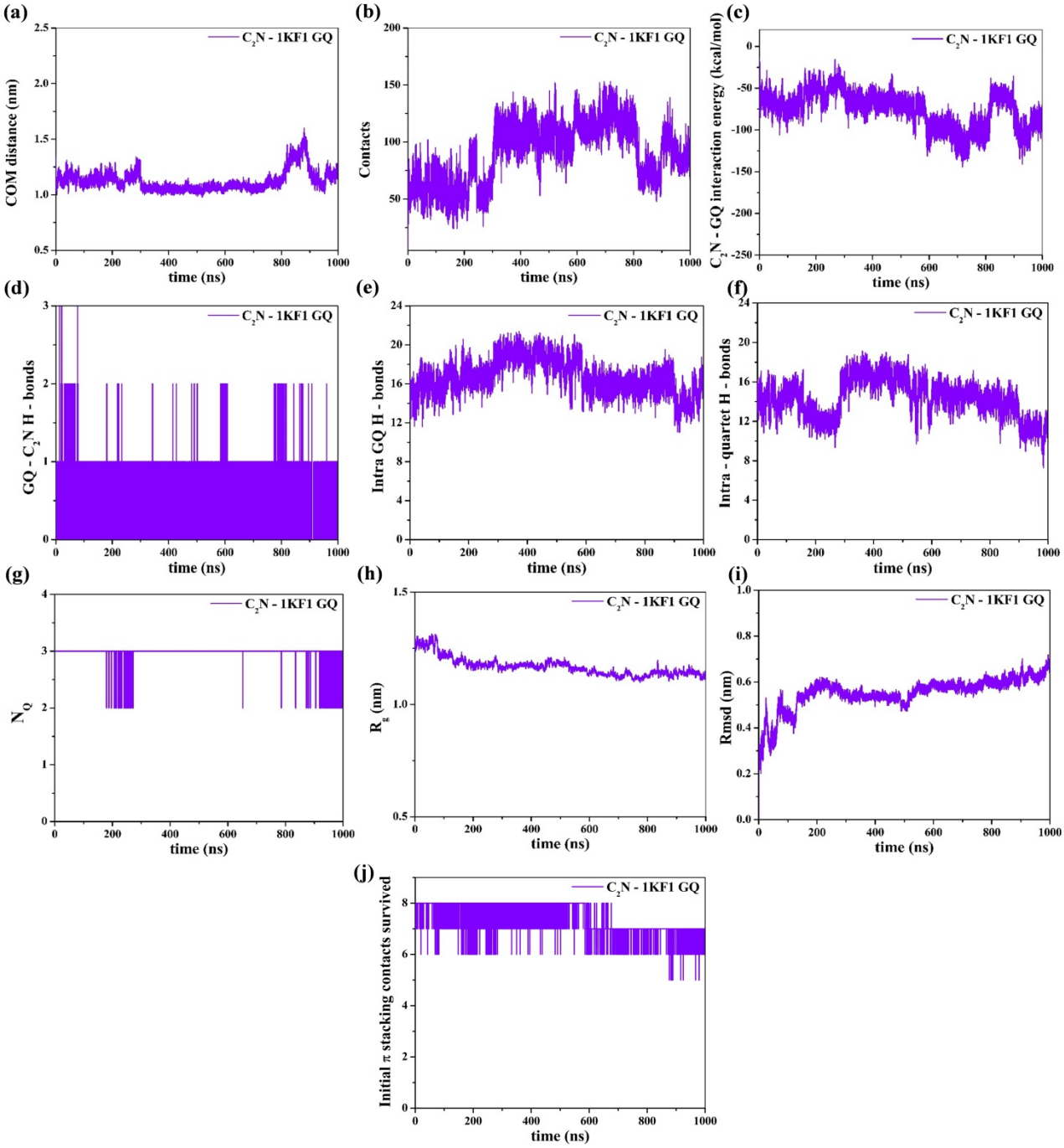

Figure S9: *Time evolution of detailed dynamical quantities characterizing the adsorption of 1KF1 - GQ onto C_2N without structural perturbation, as observed from the one microsecond long production simulation: (a) COM distance, (b) number of contacts (N_c), (c) interaction energy, (d) C_2N – GQ hydrogen bonds, (e) intra – GQ hydrogen bonds, (f) intra – quartet*

hydrogen bonds, (g) number of survived quartet motifs, (h) radius of gyration (R_g), (i) backbone root mean squared displacement (RMSD) and (j) survived π stacking contacts between nucleobases.

11. Results of the simulations of 1KF1 – GQ on C_2N with modified parameters for Nitrogen atoms:

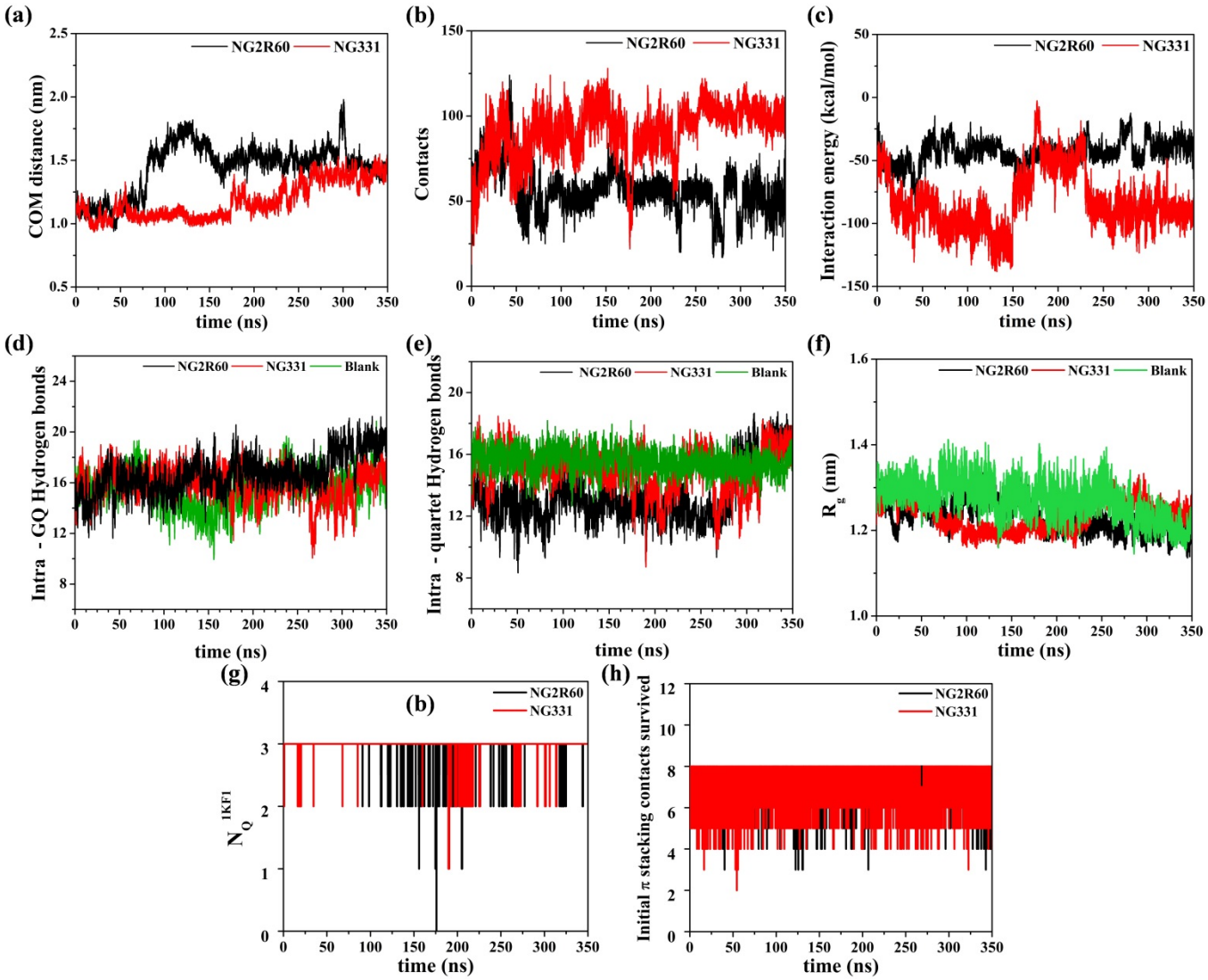

Figure S10: *Time evolution of various dynamical quantities characterizing the adsorption of 1KF1 - GQ onto 2D materials using two different parameters for C_2N nitrogen atoms namely NG2R60 and NG331 respectively: (a) COM distance, (b) number of contacts (N_c), (c) interaction*

energy, (d) intra – GQ hydrogen bonds, (e) intra – quartet hydrogen bonds, (f) radius of gyration (R_g), (g) number of survived quartet motifs and (h) survived π stacking contacts between nucleobases.

12. Analyses of the second set of adsorption simulation of 1KF1 – GQ on all three 2D materials:

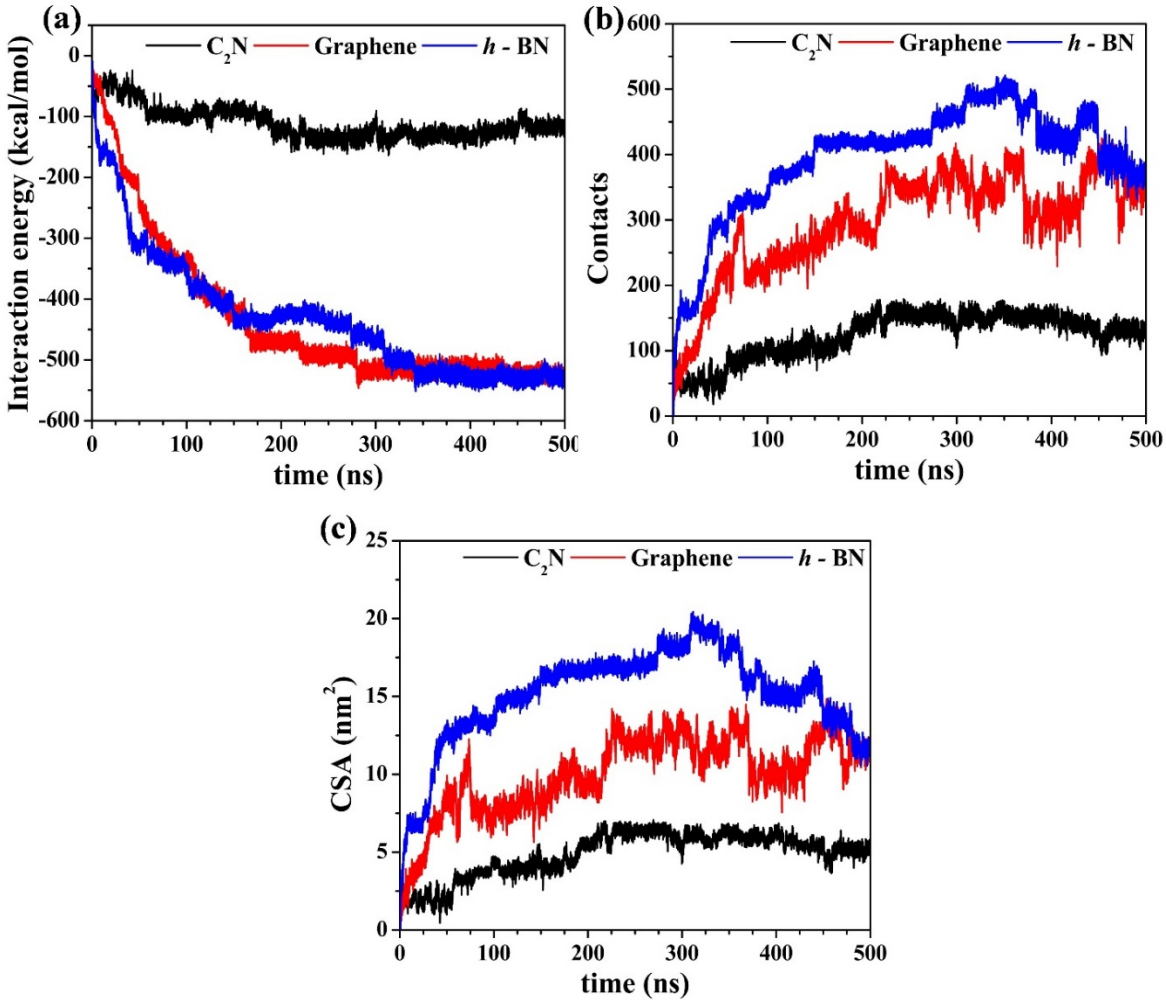

Figure S11: *Time evolution of detailed dynamical quantities characterizing the adsorption of 1KF1 - GQ onto C_2N, as observed from the second set of 500ns long production simulation: (a) interaction energy, (b) number of contacts (N_c), (c) contact surface area.*

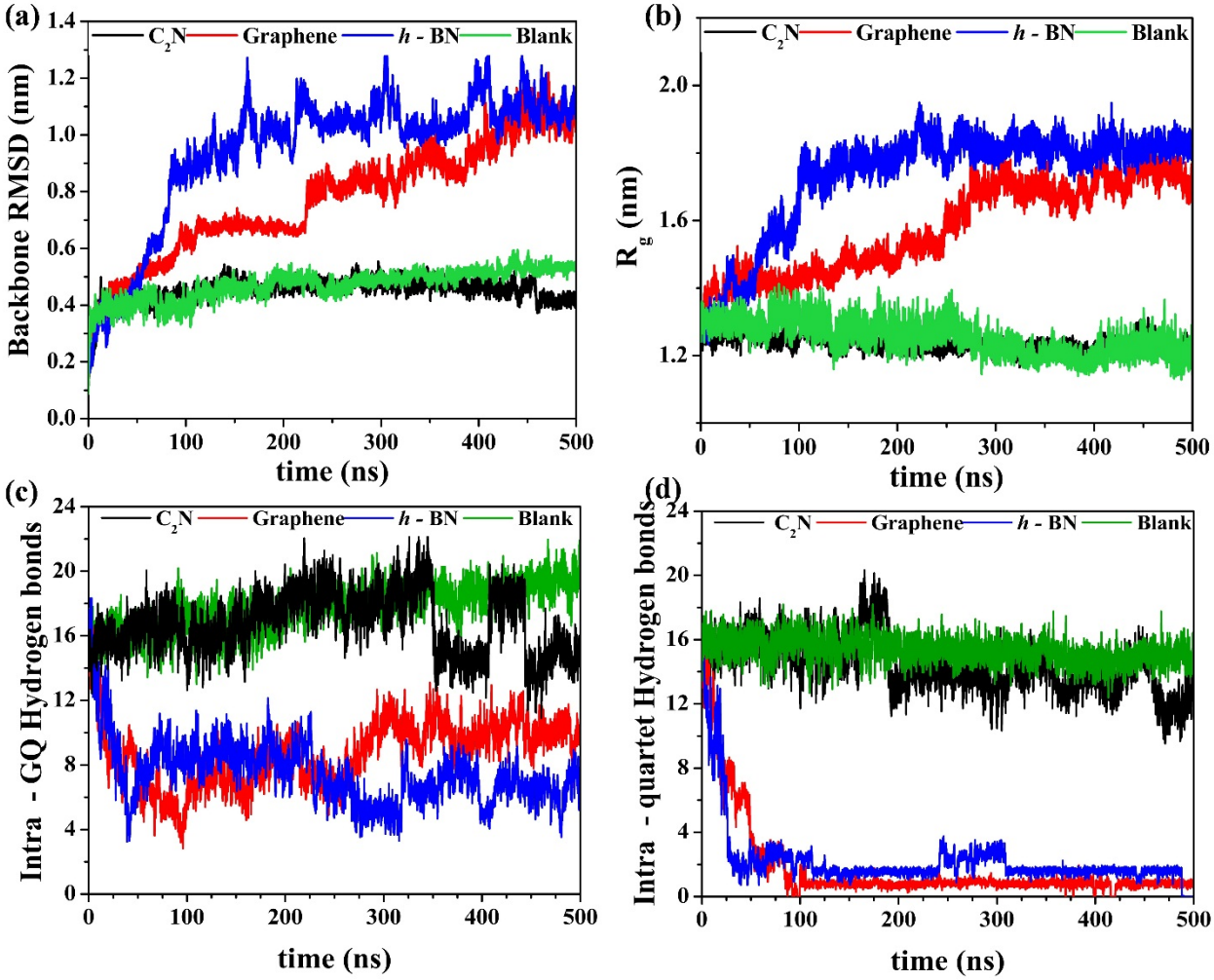

Figure S12: *Time evolution of detailed dynamical quantities characterizing the structural evolution of 1KF1 - GQ onto C_2N, as observed from the second set of 500ns long production simulation: (a) backbone RMSD, (b) radius of gyration (R_g), (c) intra – GQ hydrogen bonds and (d) intra – quartet hydrogen bonds.*

13. Snapshots for the adsorption of 1KF1-GQ on graphene and h-BN at 300 K showing quartet disruptions:

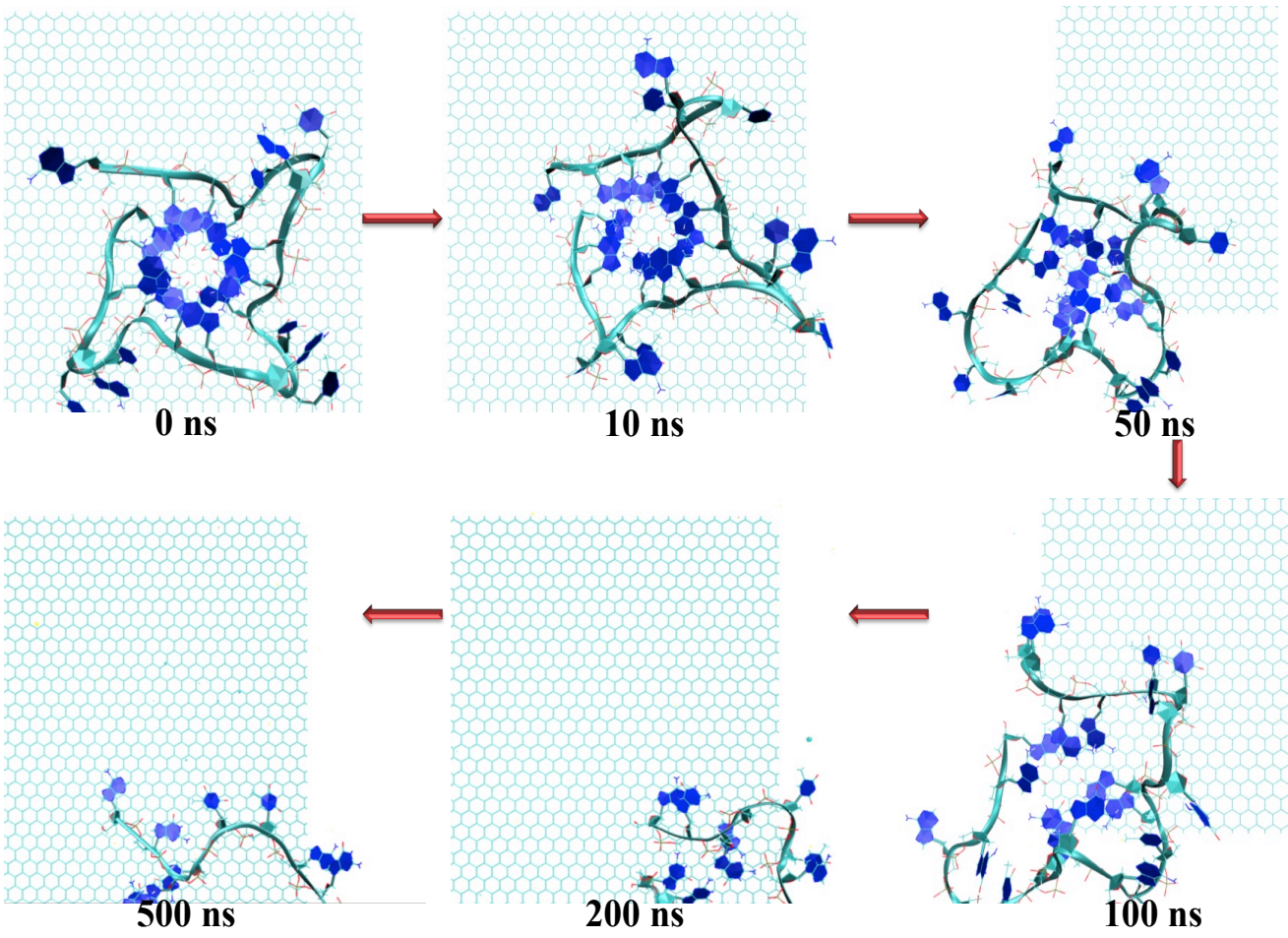

Figure S13: *Snapshots for the adsorption of 1KF1-GQ on graphene at 300 K at different time instants showing disruption of the central quartet channel within only 50 – 70 ns.*

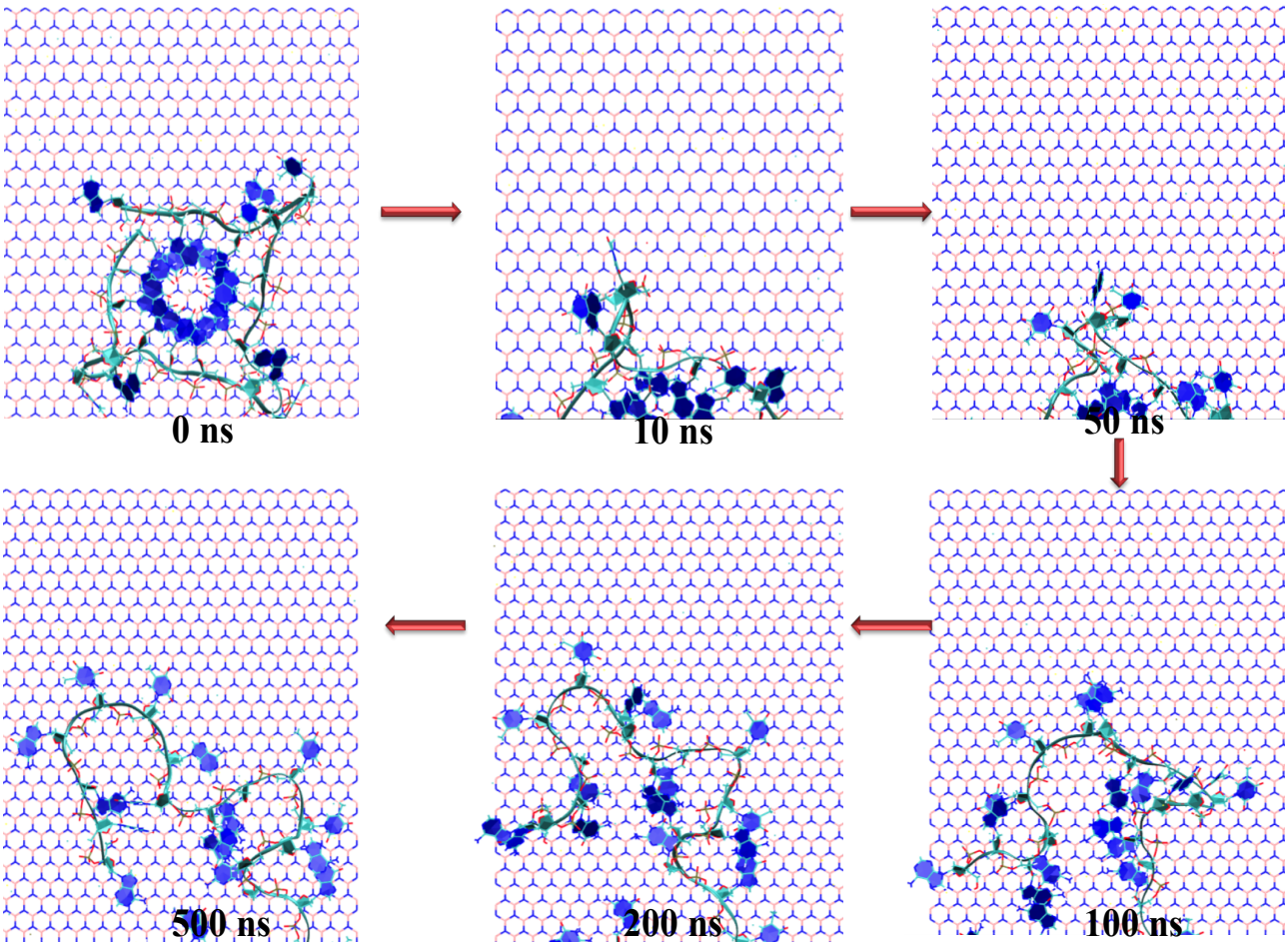

Figure S14: *Snapshots for the adsorption of 1KF1-GQ on hexagonal boron nitride at 300 K at different time instants showing disruption of the central quartet channel within only 100 ns.*

14. Snapshots for the adsorption of 143D-GQ on C_2N, grpahene and h-BN respectively at 300 K:

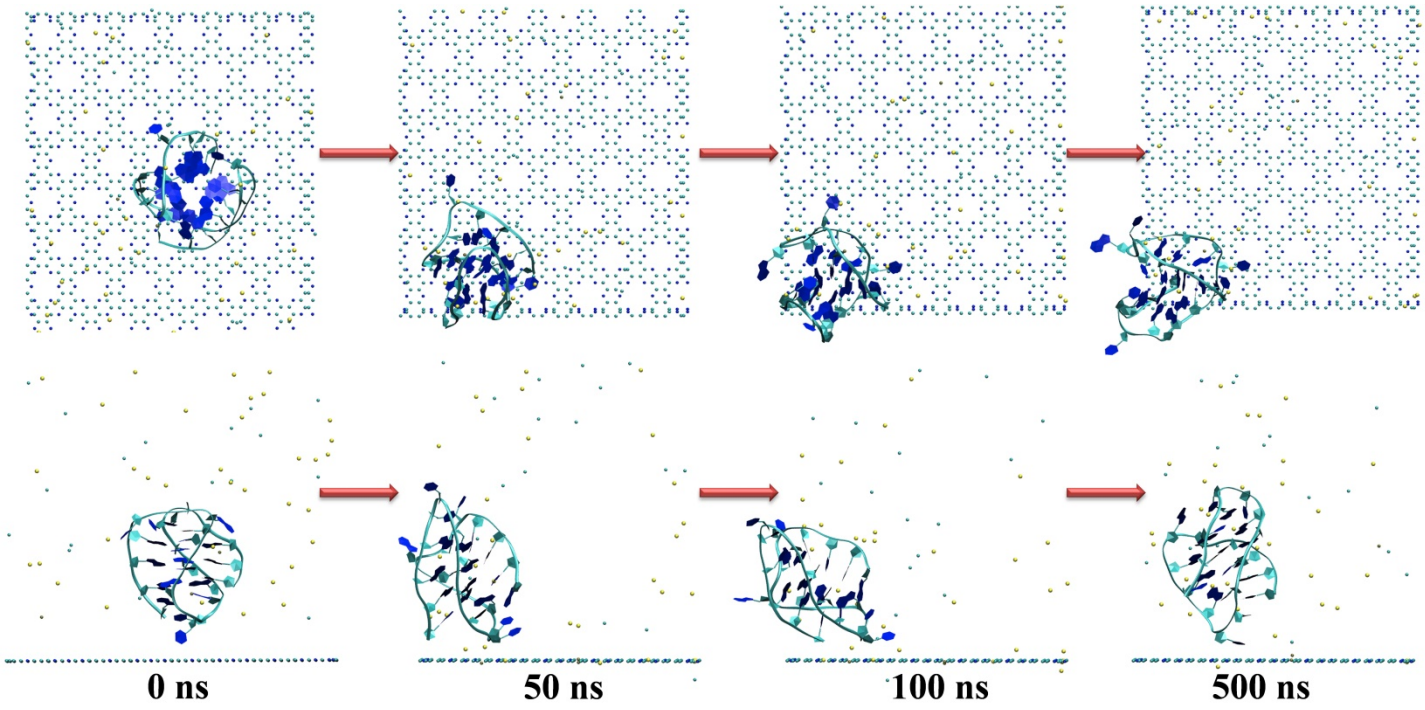

Figure S15: *Snapshots for the adsorption of 143D-GQ on C_2N at 300 K at different time instants showing the stable quartet channel within even after 500 ns.*

Figure S16: *Snapshots for the adsorption of 143D-GQ on graphene at 300 K at different time instants showing quartet disruption.*

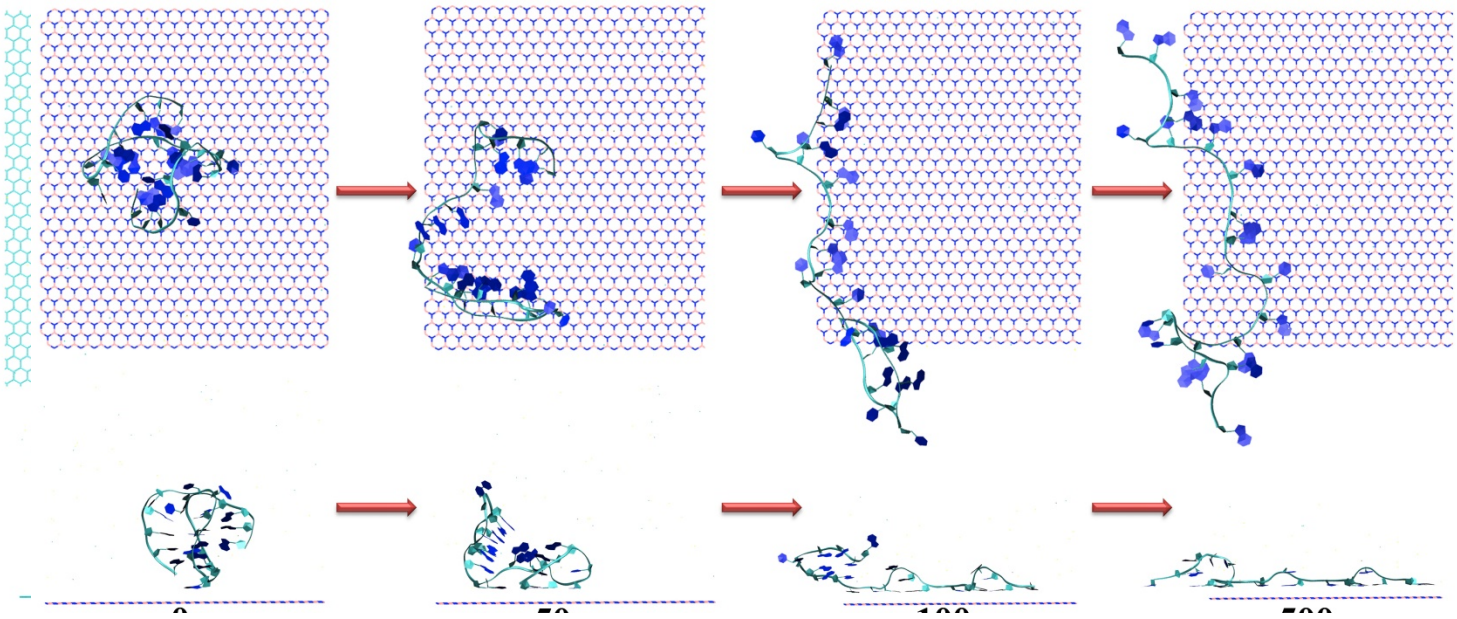

Figure S17: *Snapshots for the adsorption of 143D-GQ on h-BN at 300 K at different time instants showing quartet disruption.*

15. Analyses of the adsorption simulation of 143D – GQ on all three 2D materials:

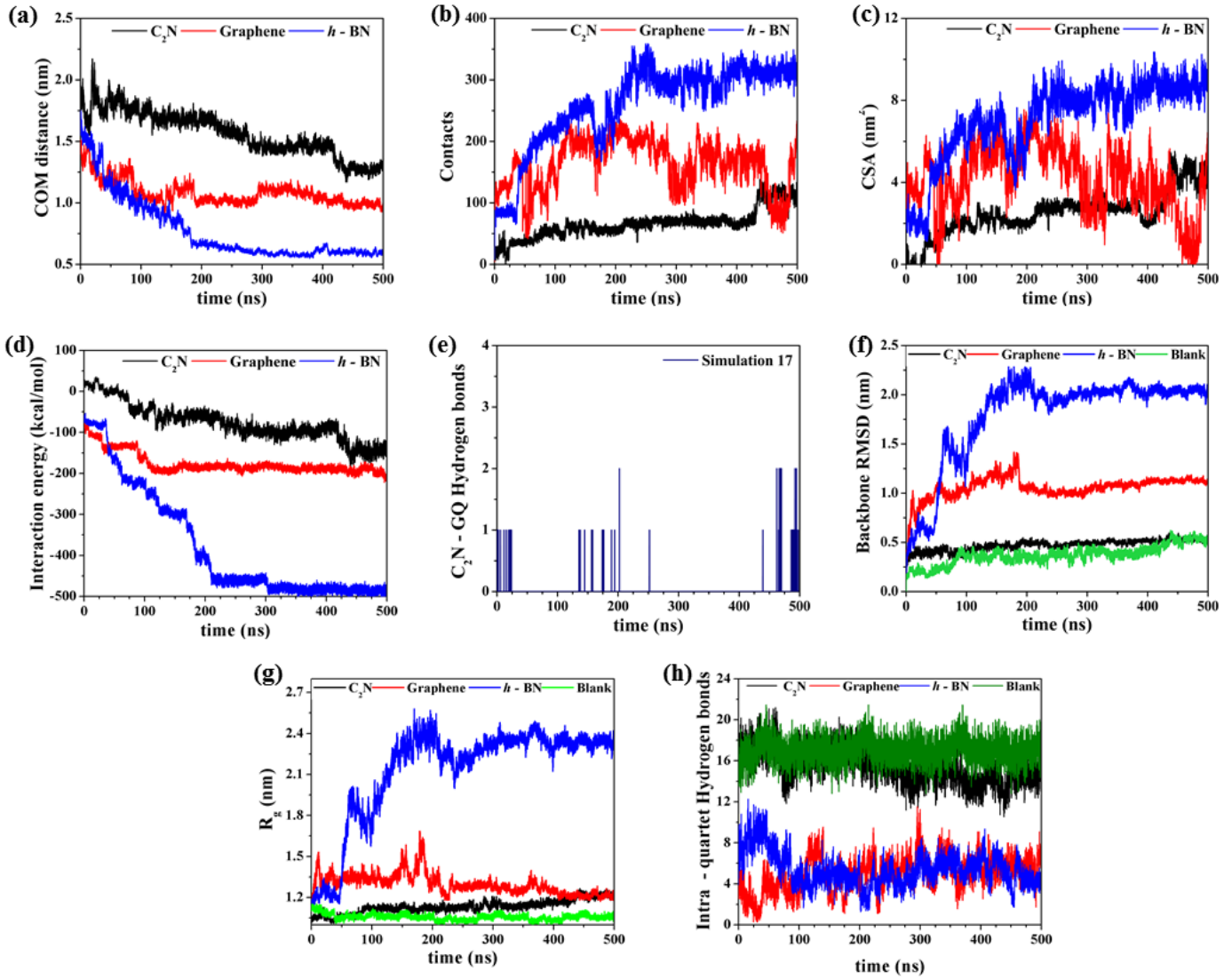

Figure S18: *Time evolution of detailed dynamical quantities characterizing the adsorption of 143D - GQ on all three 2D materials and evolution of the nucleic acid secondary structure, as observed from the 500 ns long production simulation at 300 K: (a) COM distance, (b) number of contacts (N_c), (c) contact surface area (CSA), (d) interaction energy, (e) C_2N – GQ hydrogen bonds, (f) backbone root mean squared displacement (RMSD), (g) radius of gyration (R_g) and (h) intra – GQ hydrogen bonds.*

16. Effect of ions on nucleic acid adsorption:

To probe into the behavior of ions in the immediate vicinity of the nucleic acids, we have plotted the radial distribution functions (g(r)) between two selected nucleic acids namely dsDNA and GQ-1KF1 and Na^+ as well as Cl^- ions (Figure S17(a-d)), for the pure nucleic acid system (blank) and also for all three 2D materials. As seen from Figure S17(a) and S17(b), several peaks for the presence of Na^+ ions are observed between 0.2-0.5nm, the first appearing around 0.2nm. These peak positions are characteristic for all nucleic acids as seen from the blank simulations and correspond to the attractive electrostatic interactions between the phosphate backbone of the nucleic acids and counter ions. It should be noted that, for the adsorbed nucleic acids on 2D materials, we observe the peaks corresponding to Na^+ to increase significantly, which is due to the restricted movement of nucleic acids on 2D materials, giving opportunity to the ions for condensation around the nucleic acids. On the other hand, due to intrinsic repulsion with Cl^- ions, the probability of finding the anions near the nucleic acids are indeed low, much lower compared to the bulk, as observed from Figure S17(c) and S17(d). However, unlike the case of Na^+, the adsorbed nucleic acids being restricted to move, constantly repel the Cl^- ions, thereby further excluding the anions from the neighborhood and decreasing the corresponding probability of finding. Also, in order to shed light into the surface effects on ion condensation, we plotted the plotted the radial distribution functions (g(r)) between the three surfaces and Na^+ as well as Cl^- ions (Figure S18(a-d)) respectively. It is clearly seen that, due to the charge localization on C_2N unlike graphene and *h*-BN, both Na^+ and Cl^- ions appear at a closer distance during the interaction with the former compared to the latter. While both the ions do not have any well-defined peak in the g(r) plots with graphene and *h*-BN, proper layering is observed for C_2N suggesting significantly strong surface – ion interactions. In fact we observe few Na^+ ions to be trapped within the pores on C_2N surface, which are surrounded by negatively charged N atoms of

the surface pyrazine rings, which has been reported in articles concerned with water desalination techniques using C_2N. Nevertheless, the surface-ion interactions are not expected to affect the interactions with nucleic acids since the nucleic acid-ion g(r) plots are very similar to those observed in pure water. As a whole, adsorption on 2D materials tend to favor the nucleic acid-cation interactions while anions get repelled more efficiently, although keeping the nature DNA-ion interactions very similar to that observed in absence of 2D materials.

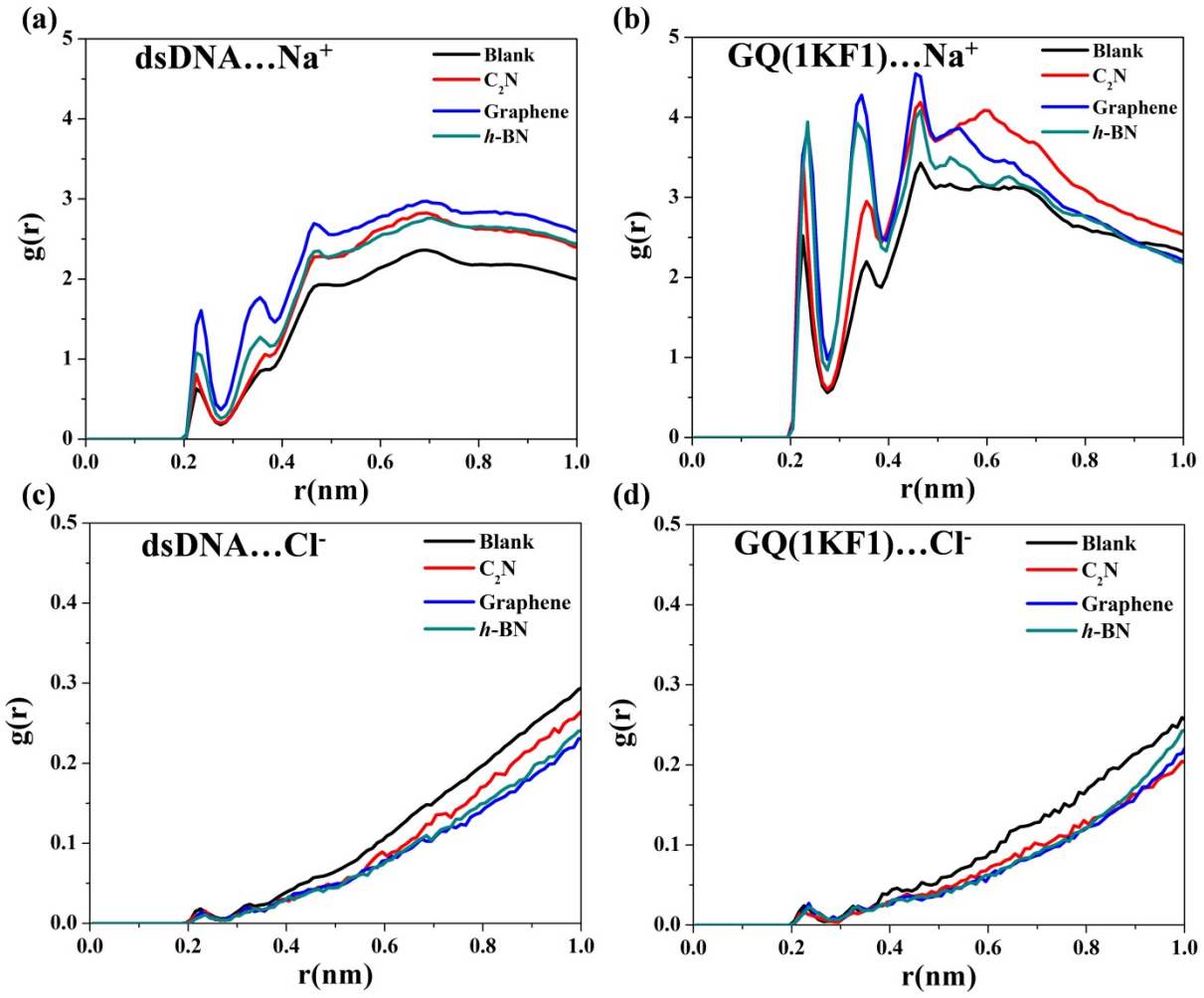

Figure S19: *Radial distribution functions between a dsDNA and GQ (1KF1) with (a,b) sodium (Na^+) and (c,d) chloride (Cl^-) ions respectively for the pure nucleic acid (blank) and the adsorbed nucleic acids in presence of all three 2D materials.*

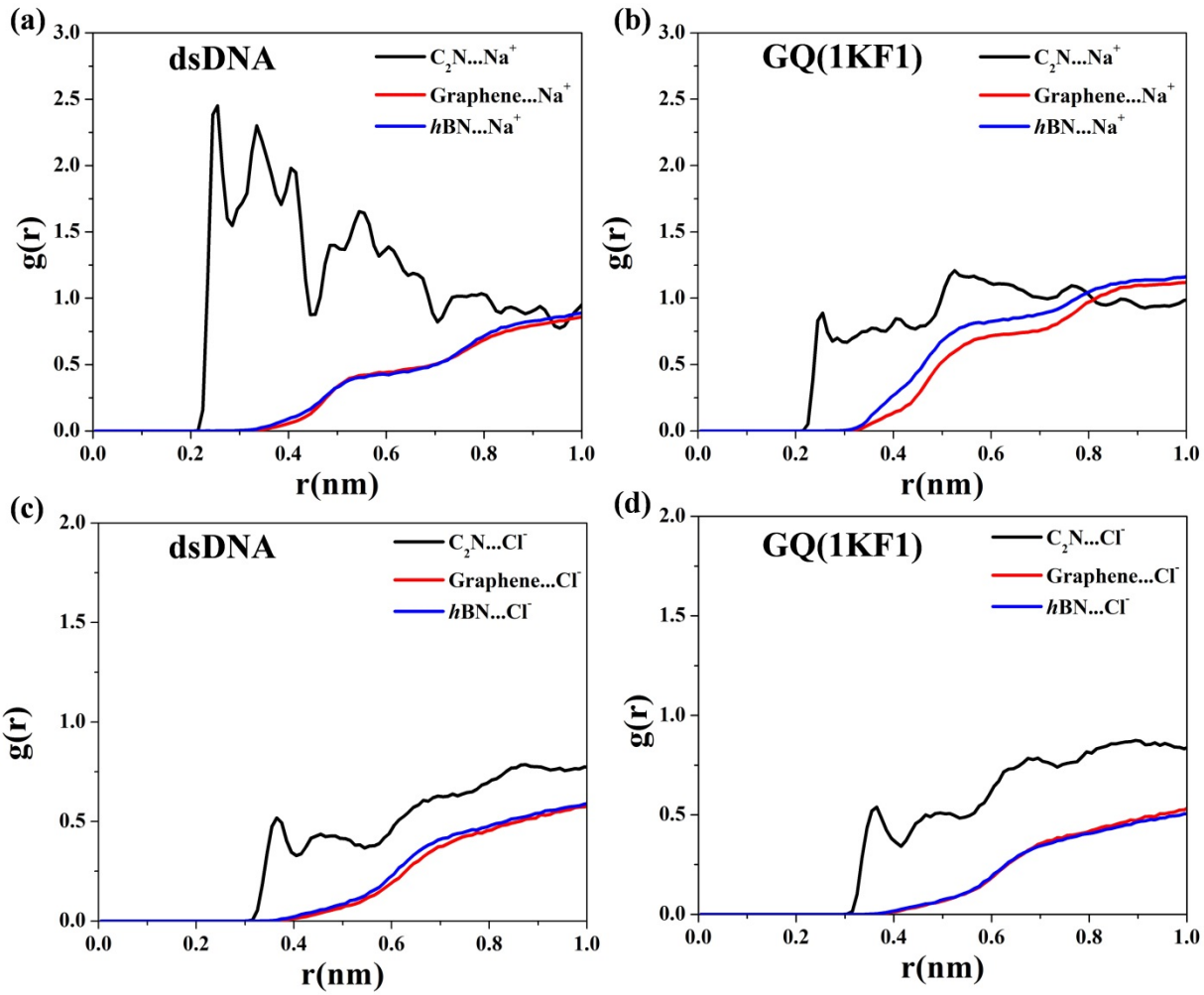

Figure S20: *Radial distribution functions between all three surfaces with (a,b) sodium (Na^+) and (c,d) chloride (Cl^-) ions respectively for two selected nucleic acids namely dsDNA and GQ(1KF1).*

17. Nature of nucleic acid – water Interactions:

In order to identify the effect of nucleic acid-water interactions, we have plotted the time evolution of the interaction energies and decomposed it into two components namely electrostatic and van der Waals. Two different nucleic acids are chosen, namely GQ(1KF1) and dsDNA (Figure S19(a-b) and S20(a-b) respectively). As clearly observed, both types of interaction energies remain nearly unchanged throughout the simulations, however, within the first few nanoseconds of adsorption, some interaction energy is lost, probably due to the simultaneous dehydration of the surface as well as the polynucleotides. After adsorption, there is no significant change in the time evolutions and in fact, the magnitudes of the interaction energies are very similar to that observed when none of the 2D materials is present. Therefore, except for the nanoscale dewetting of C_2N during initial stages of adsorption, water molecules do not significantly interfere with the process. However, again it is due to the polar nature and charge localization on C_2N that the surface-water interactions are much higher than predominantly hydrophobic graphene as well as *h*-BN and therefore, dehydration leads to somewhat loss in solvation for the surface which is compensated by interacting with the polynucleotide. The above two process run in opposing direction, making the overall binding weaker. Graphene and h-BN, on the other hand, do not suffer from a large surface-water interaction energy during dewetting, thereby making the adsorption of nucleic acids largely exergonic.

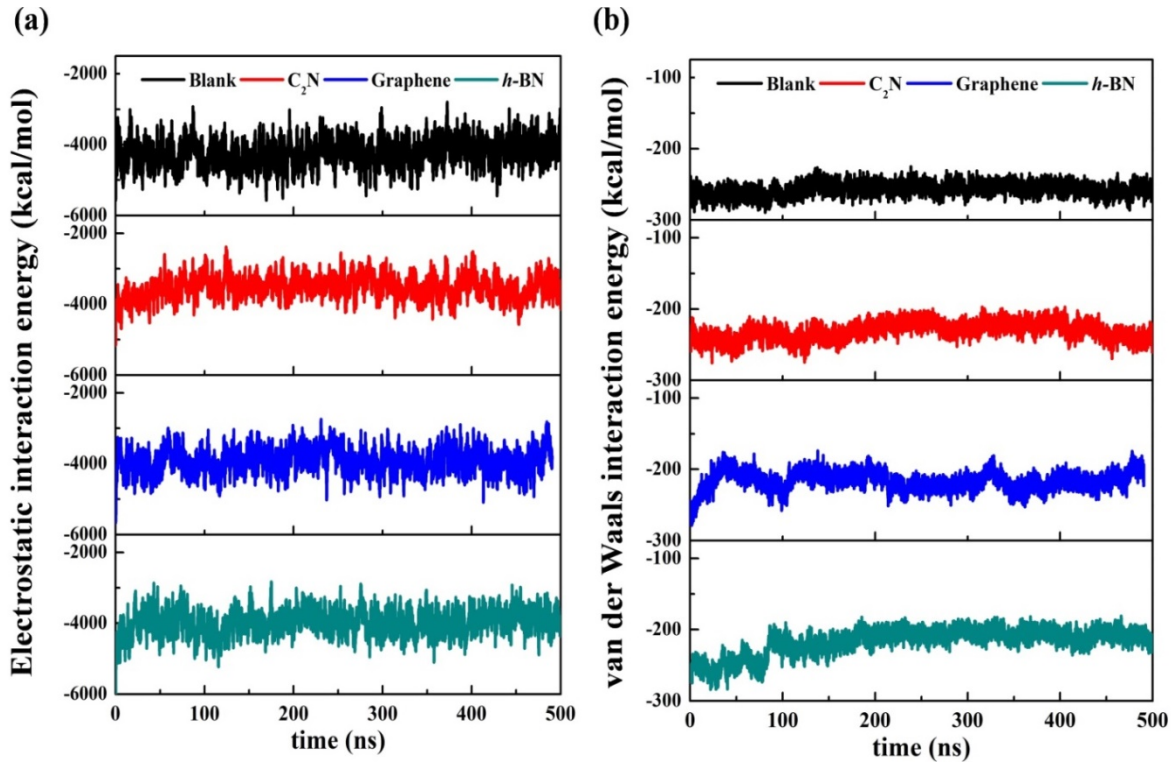

Figure S21: *Time evolution of the decomposition of GQ (1KF1)-water interaction energy into (a) electrostatic and (b) van der Waal components for the pure system without any material and for the adsorption on all three 2D materials.*

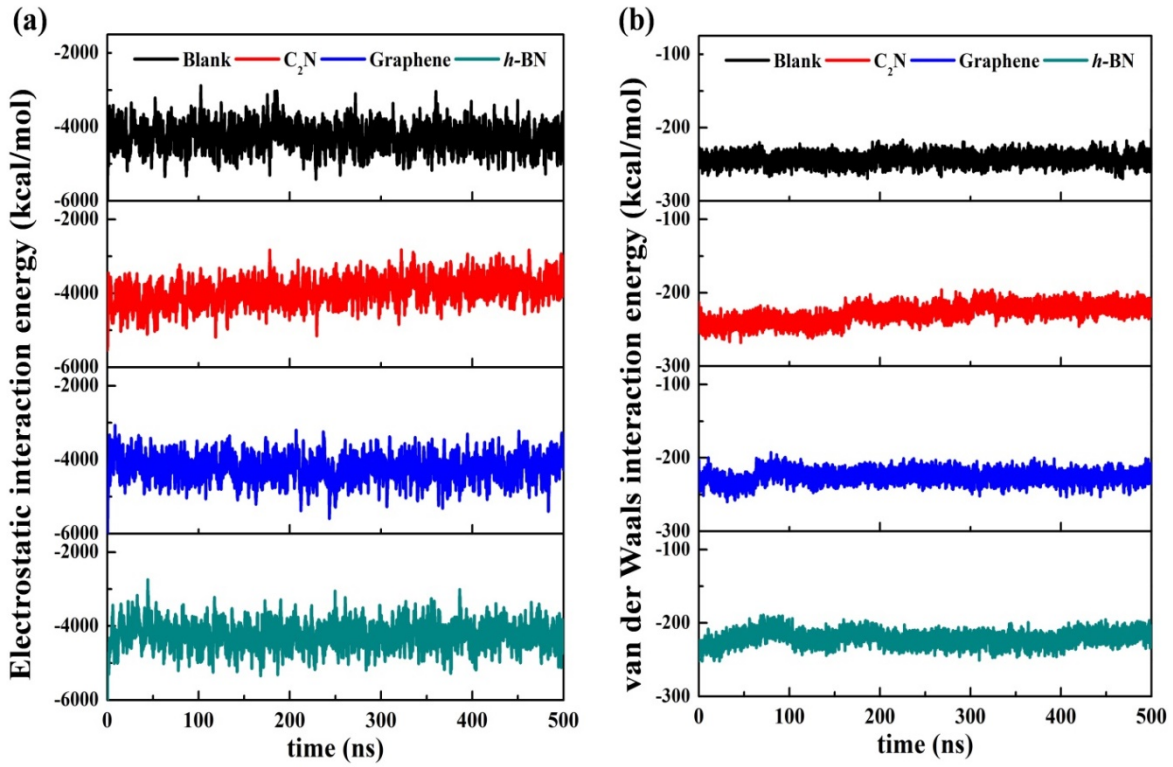

Figure S22: *Time evolution of the decomposition of dsDNA-water interaction energy into (a) electrostatic and (b) van der Waal components for the pure system without any material and for the adsorption on all three 2D materials.*

18. Analyses of normalized dynamical properties during DNA adsorption on 2D materials:

We have plotted the normalized values of some dynamical quantities during DNA adsorption on the 2D materials in Figure S21(a-c) and S22(a-c) by dividing the quantities with the number of atoms in the nano-sheets for two different systems namely dsDNA and the GQ (1KF1) respectively. As observed from the figures, the trends in the quantities remain nearly the same as that before normalization, clearly demonstrating the fact that the binding of polynucleotides with C_2N is certainly weaker compared to graphene and *h*-BN. Since, two of the nucleic acids used in this study resemble the same trend, we expect other nucleic acids such as ssDNA and UBP containing DNA's to follow similar patterns.

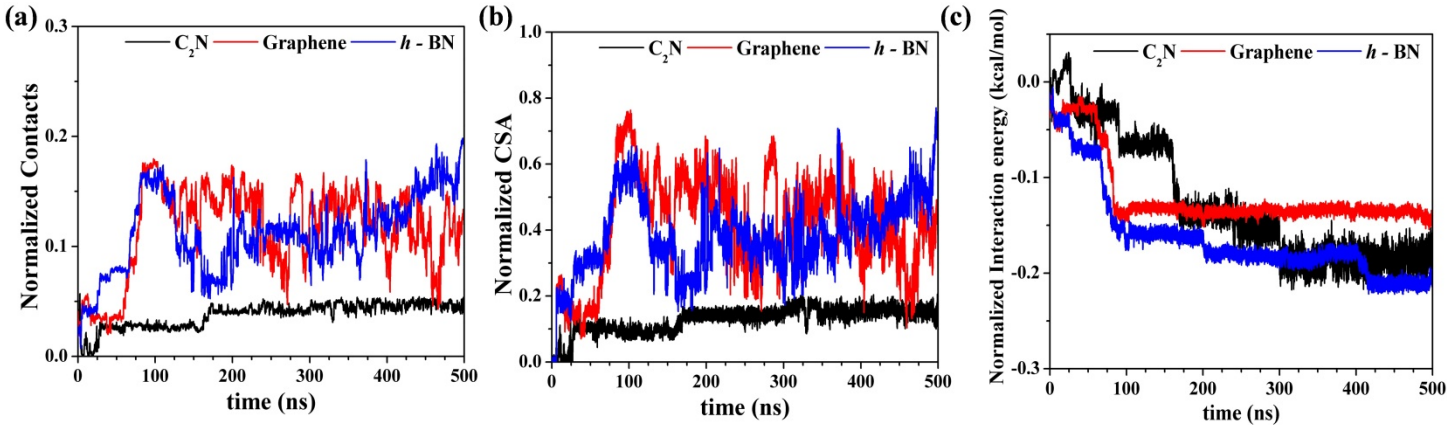

Figure S23: *Time evolution of normalized dynamical quantities characterizing the adsorption of a dsDNA onto C_2N, graphene and h – BN: (a) number of contacts (N_c), (b) contact surface area and (c) interaction energy.*

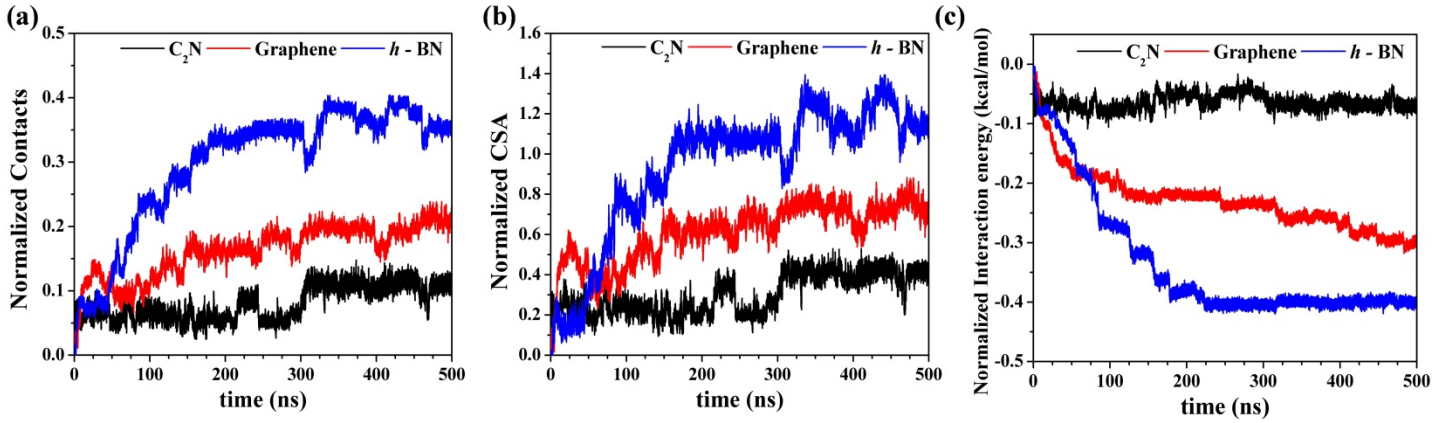

Figure S24: *Time evolution of normalized dynamical quantities characterizing the adsorption of a guanine quadruplex (GQ-1KF1) onto C_2N, graphene and h – BN: (a) number of contacts (N_c), (b) contact surface area and (c) interaction energy.*

19. Accuracy of simulations and comparison with AMBER parameters:

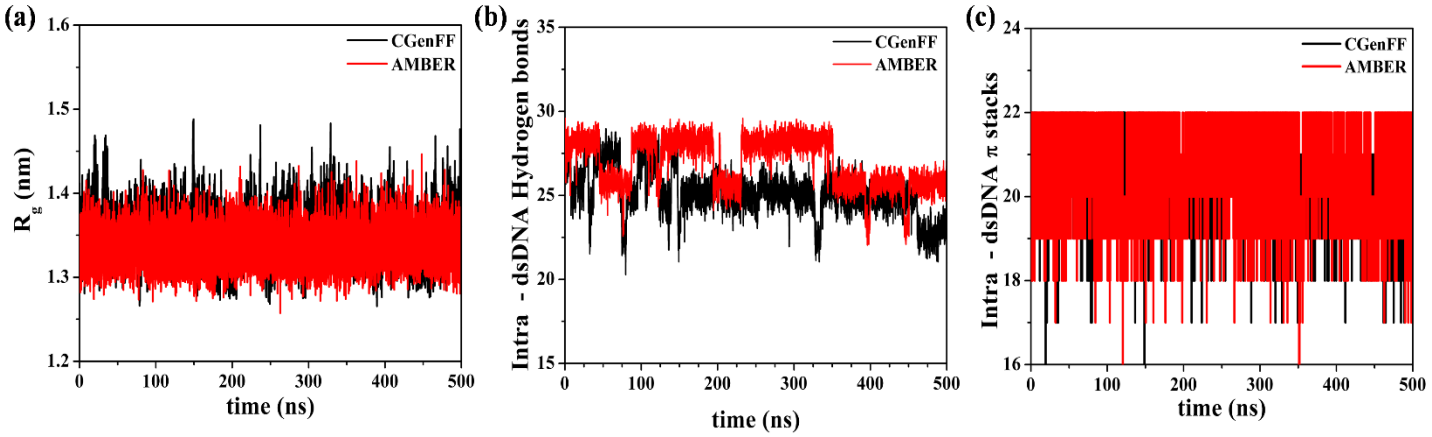

Figure S25: *Comparison of different dynamical structural properties of a dsDNA using CHARMM (CGenFF) and AMBER (parmbsc1) parameters: (a) radius of gyration (R_g), (b) intra-dsDNA H-bonds and (c) intra-dsDNA π-π stacking contacts at 300 K.*

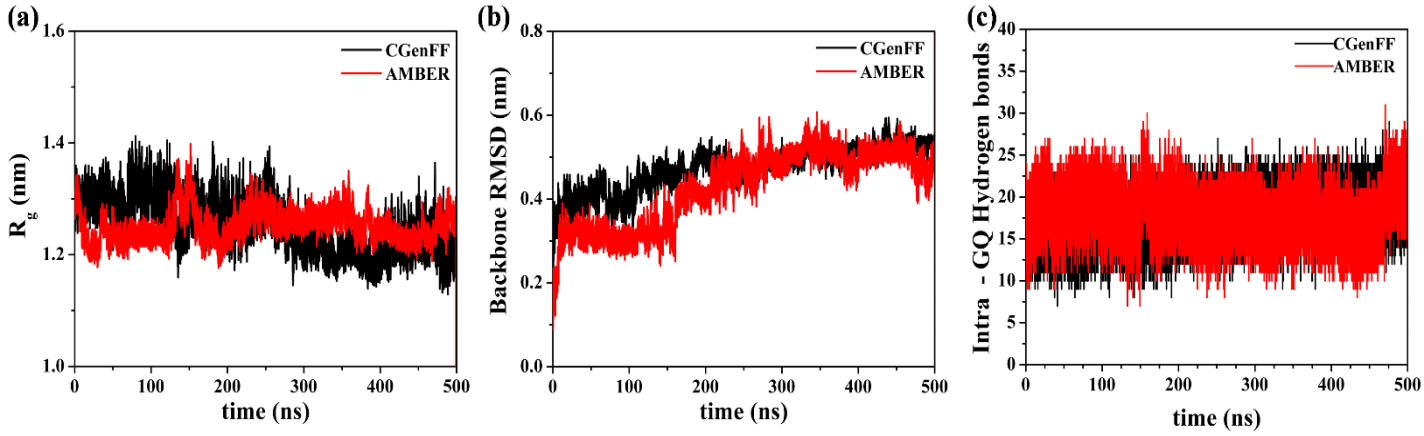

Figure S26: *Comparison of different dynamical structural properties of a dsDNA using CHARMM (CGenFF) and AMBER (parmbsc1) force-field parameters: (a) radius of gyration (R_g), (b) intra-dsDNA H-bonds and (c) intra-dsDNA π-π stacking contacts at 300 K.*

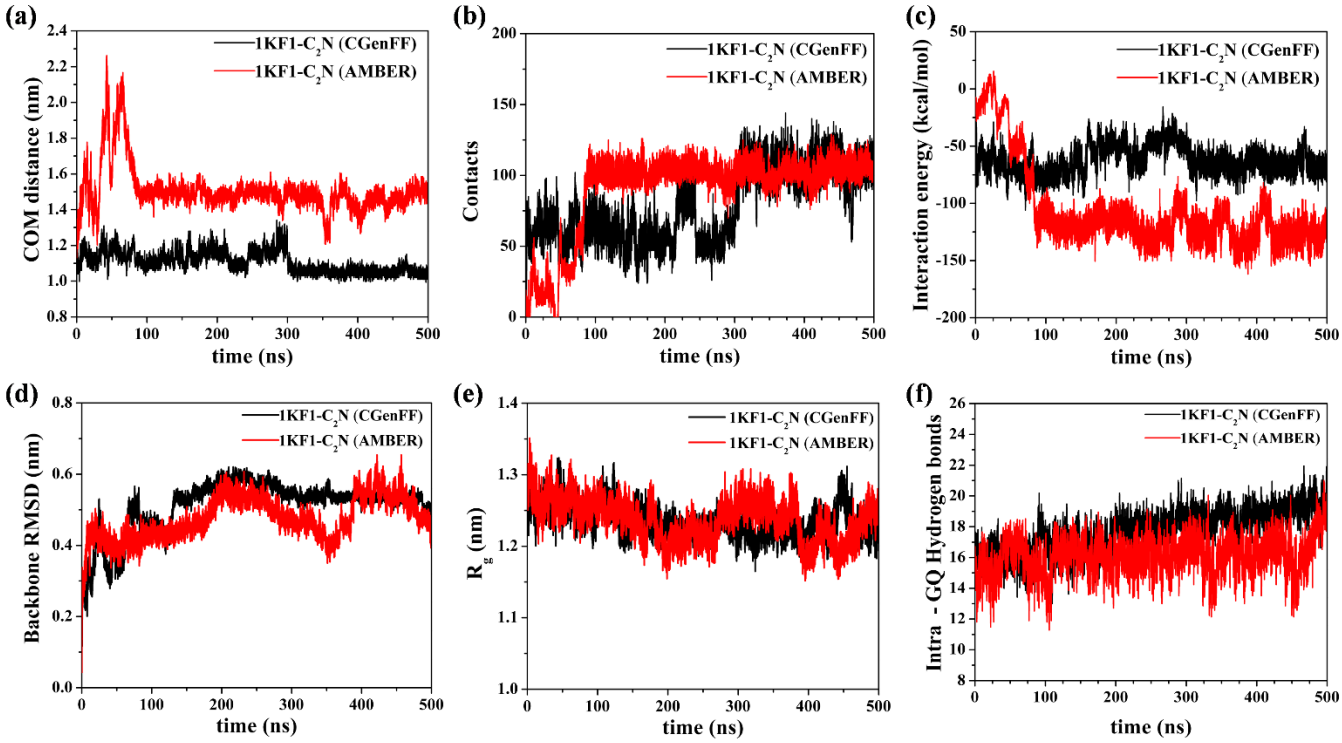

Figure S27: *Comparison of different dynamical properties of a GQ (1KF1) adsorption on C_2N using CHARMM (CGenFF) and AMBER (parmbsc1) force-field parameters at 300 K: (a) COM distance between the nucleic acid C_2N, (b) number of contacts, (c) GQ-C_2N interaction energy, (d) backbone RMSD of the GQ, (e) radius of gyration (R_g) and (f) intra-GQ H-bonds.*

20. Principal Component Analysis of the dsDNA and GQ adsorption on 2D materials:

We have carried out dihedral angle Principal component analysis (dPCA) based on the glycosidic dihedral angle (χ) which characterizes the relative base-sugar orientation for the dsDNA and GQ (1KF1) in water as well as after adsorption on all three 2D materials. To determine the dPCA, we have used sin and cosine transformed dihedral angles instead of using the dihedral angles directly and these are considered as order parameters for the structural changes of the DNA helices. Figure S28 and S29 represent the multidimentional free energy landscapes for dsDNA and GQ respectively. It is observed that, in absence of any 2D materials in water, the free energy landscapes contain two minima of which one is predominantly of lower free energy and probably the other one results from flexibility and reorganization of the

molecules in water (Figures S28(a) and S29(a)). For the adsorption on C_2N, all of these properties of the dPCA plots are maintained suggesting little to no distortion of the glycosidic dihedral angles, which in turn gives confirmation regarding the preservation of structural properties of the nucleic acids along with their conformational stability (Figures S28(b) and S29(b)). On the other hand, when adsorbed on graphene and *h*-BN, for both the DNA types, the free energy landscapes become highly rugged (Figures S28(c-d) and S29(c-d)), thereby suggesting significant spatial deviation of the sugar-base arrangements which is strongly supported by other analyses presented in the present manuscript. It should be noted that, on graphene and *h*-BN, none of clusters in the free energy landscapes is profoundly populated,

suggesting absence of any stable conformation during adsorption unlike the cases of water and adsorption on C2N, which is also in good agreement with the increase in contacts between

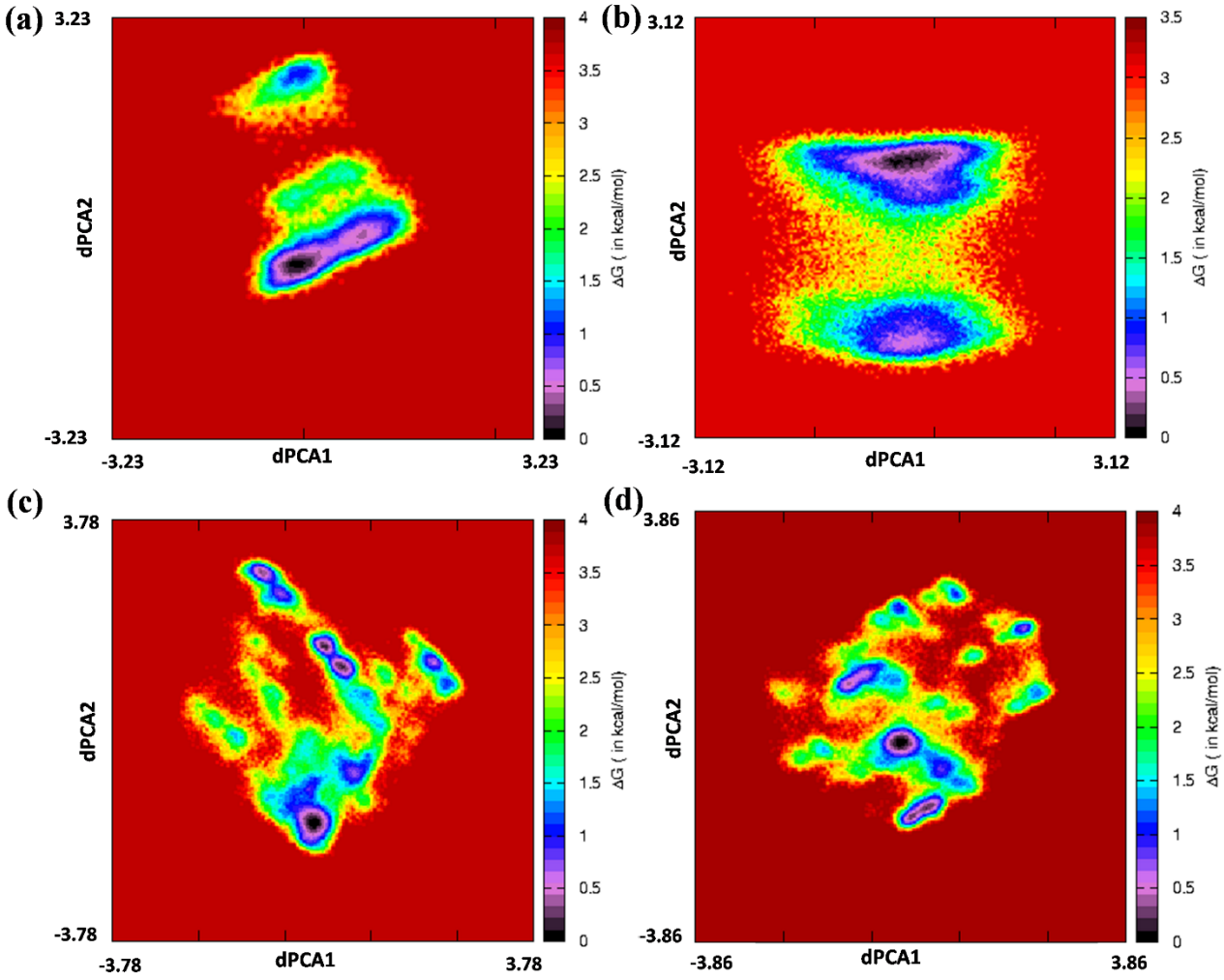

various nucleic acids with these 2D materials even after few hundred nanoseconds of adsorption simulations.

Figure S28: *Free energy landscapes regarding the dihedral principal component analysis (dPCA) for dsDNA in (a) water and on (b) C_2N, (c) graphene and (d) h-BN during the adsorption simulations at 300K. The dPCA is carried out using the glycosidic dihedral angle (χ) which characterizes the relative base-sugar orientation for any nucleic acid. To determine the dPCA, we have used sin and cosine transformed dihedral angles instead of using the dihedral*

angles directly and these are considered as order parameters for the structural changes of the DNA helices.

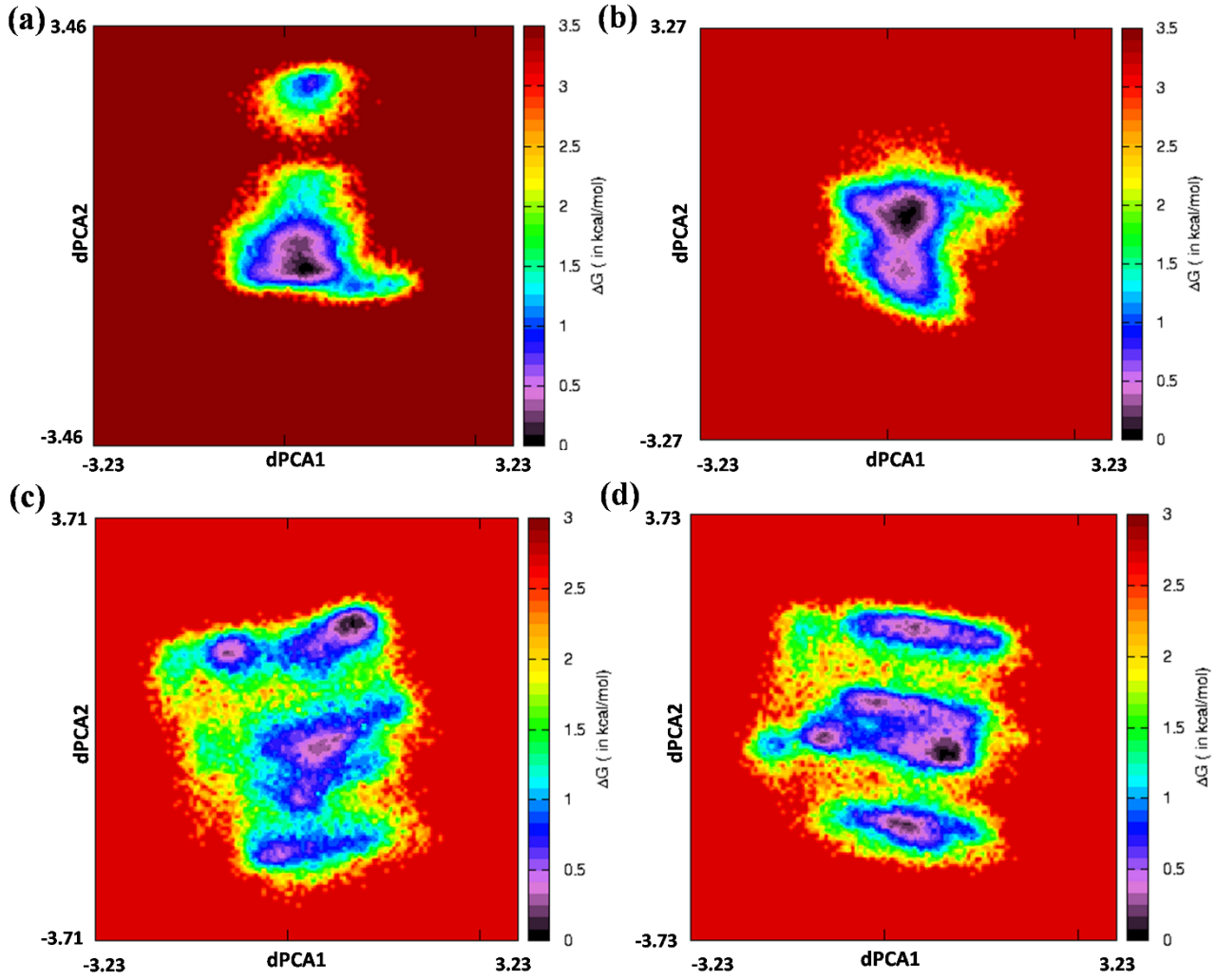

Figure S28: *Free energy landscapes regarding the dihedral principal component analysis (dPCA) for GQ-1KF1 in (a) water and on (b) C_2N, (c) graphene and (d) h-BN during the adsorption simulations at 300K. The dPCA is carried out using the glycosidic dihedral angle (χ) which characterizes the relative base-sugar orientation for any nucleic acid. To determine the dPCA, we have used sin and cosine transformed dihedral angles instead of using the dihedral*

angles directly and these are considered as order parameters for the structural changes of the DNA helices.

References:

(1) Malyshev, D. A.; Dhami, K.; Lavergne, T.; Chen, T.; Dai, N.; Foster, J. M.; Corrêa, I. R.; Romesberg, F. E. A semi-synthetic organism with an expanded genetic alphabet. *Nature* **2014**, *509*, 385.

(2) Jahiruddin, S.; Datta, A. What Sustains the Unnatural Base Pairs (UBPs) with No Hydrogen Bonds. *The Journal of Physical Chemistry B* **2015**, *119*, 5839-5845.

(3) Kimoto, M.; Yamashige, R.; Matsunaga, K.-i.; Yokoyama, S.; Hirao, I. Generation of high-affinity DNA aptamers using an expanded genetic alphabet. *Nature Biotechnology* **2013**, *31*, 453.

(4) Jahiruddin, S.; Mandal, N.; Datta, A. Structure and Electronic Properties of Unnatural Base Pairs: The Role of Dispersion Interactions. *ChemPhysChem* **2018**, *19*, 67-74.